

# Dispersion compensation in whispering-gallery modes

Vladimir S. Ilchenko, Anatoliy A. Savchenkov, Andrey B. Matsko, and Lute Maleki

*Jet Propulsion Laboratory, California Institute of Technology, 4800 Oak Grove Drive,  
Pasadena, California 91109-8099*

Received May 29, 2002; revised manuscript received July 31, 2002; accepted August 9, 2002

We show that manipulation by a spatial profile of the refractive index of a circularly symmetric dielectric cavity results in a novel way of fine tuning frequency separations as well as spatial localizations of high- $Q$  whispering-gallery modes excited in the cavity. The method permits dispersion compensation in the modes (spectrum equalization), diminishes the quality-factor limitation by surface roughness and contamination, and allows critical coupling to ultra-high- $Q$  modes without maintaining an air gap with evanescent couplers.

© 2003 Optical Society of America

OCIS codes: 230.5750, 260.2030, 230.1150, 220.4830.

## 1. INTRODUCTION

Optical cavities consisting of two or more mirrors are utilized in all branches of modern linear and nonlinear optics. Practical usage of such cavities is technically restricted, especially when high performance of the devices, i.e., a high quality factor and high mode stability, is important. Fabrication of good optical mirrors, their alignment, and binding are rather expensive and difficult tasks.

Open dielectric microcavities may become an alternative for the usual optical cavities. Fabrication of these microcavities is rather simple and inexpensive. The cavities demonstrate high mode stability and high quality factors. High- $Q$  optical microcavities with whispering-gallery modes (WGMs)<sup>1–4</sup> are already in the core of many evolving photonics applications from high-stability narrow-linewidth microlasers,<sup>5–15</sup> high-resolution spectroscopy, remote sensing, and optoelectronic oscillators<sup>16–22</sup> to optical memory devices, true-time optical delay lines, and optical switching devices.<sup>23–27</sup>

However, there are significant differences between properties of open dielectric microcavities and conventional optical cavities constructed of mirrors. Originally proposed spherical WGM microcavities (microspheres) are overmoded, with complex quasi-periodic spectra and unequal mode spacings translating from both material and cavity dispersion. Significant reduction in the mode spectral density is achieved in a highly oblate spheroidal microcavity (microtorus),<sup>28</sup> but still-current fabrication technologies cannot produce dielectric microcavities with equidistant spectra.

Performance and range of applications based on WGM microcavities will be significantly expanded if a method is found to make microcavity modes equally spaced with precision corresponding to a fraction of the resonance bandwidth. Such a dielectric microcavity with an equidistant mode spectrum is similar to the Fabry–Perot resonator. A dielectric cavity with an equidistant spectrum may be used, for example, in frequency comb generators,

optical pulse generators, broadband energy-storage circuits of electro-optical devices, and in other applications in which conventional optical cavities are utilized.

Within current technology based on uniform resonator material, the smaller the cavity size is, the more the cavity dispersion is manifested in unequal spectral separation between adjacent modes. The problem is rooted in the fact that the radial distribution of whispering-gallery resonant modes is frequency dependent. Higher-frequency modes propagate on paths that are slightly closer to the surface than those of lower-frequency modes. Thus higher-frequency modes travel in trajectories of a slightly larger radius and slightly longer optical path lengths.

Optical path length is a function of both the physical distance and the index of refraction. We propose to fabricate a cavity out of a cylindrically symmetric material whose index decreases in the radial direction. With the proper choice of a gradient of the refractive index, circular trajectories corresponding to the WGM at different frequencies will have identical optical path lengths. This results in an equidistant mode spectrum of the cavity.

We show that mode confinement is also changed in a cavity made from a graded-index material.<sup>29</sup> The position of the maximum of the field of each mode shifts toward the cavity center, and mode volumes are increased and displaced away from the surface, thereby desensitizing the quality factor from the effects of surface contamination and roughness. Both of these effects are identified currently as the main factor preventing the improvement of  $Q$  toward the fundamental limit imposed by bulk-material attenuation. Therefore we predict a substantial increase of the mode quality factor in graded-index cavities.

Finally, burying the mode volume well inside the resonator helps to address the technical problem of maintaining the tunneling gap between a high- $Q$  WGM cavity and an evanescent wave coupler device. With appropriate engineering, critical coupling will be obtained under full mechanical contact with the coupler.

## 2. WHISPERING-GALLERY MODES: BASICS

Let us consider a dielectric sphere with dielectric constant distribution  $\epsilon(r)$  that depends on the radius  $r$  only. The electric field in the sphere obeys the Maxwell equation

$$\nabla \times (\nabla \times \mathbf{E}) + \frac{\epsilon(r)}{c^2} \frac{\partial^2 \mathbf{E}}{\partial t^2} = 0, \quad (1)$$

where  $c$  is the speed of light in vacuum. Presenting the electric field as  $\mathbf{E} = \int_0^\infty d\omega \mathbf{e}(r) \exp(-i\omega t)$ , we rewrite the above equation as

$$\nabla \times (\nabla \times \mathbf{e}) - k^2 \epsilon(r) \mathbf{e} = 0, \quad (2)$$

where  $k = \omega/c$  is the wave vector. Equation (2) may be solved in terms of TE and TM modes. Keeping in mind that  $\nabla \cdot (\epsilon \mathbf{e}) = 0$ , we write

$$\mathbf{e} = \sum_{\nu, m} \frac{1}{r} \left[ \Psi \mathbf{Y}_{\nu, m} + \frac{1}{\epsilon(r)} \nabla \times (\Phi \mathbf{Y}_{\nu, m}) \right], \quad (3)$$

where radial functions  $\Psi$  and  $\Phi$  stand for TE and TM modes, respectively, and  $\mathbf{Y}_{\nu, m}$  are vector spherical functions with angular number  $\nu$  and magnetic number  $m$ . It is worth noting that modes of an infinite dielectric cylinder may be described in a similar way.

Radial field distribution for TE modes<sup>30</sup> of a dielectric cavity (sphere or cylinder) can be described by the equation

$$\frac{\partial^2 \Psi}{\partial r^2} + \left[ k^2 \epsilon(r) - \frac{\nu(\nu+1)}{r^2} \right] \Psi = 0, \quad (4)$$

where  $\nu$  is the angular momentum number ( $\nu = 0, 1, 2, 3, \dots$  for a sphere and  $\nu = 1/2, 3/2, 5/2, \dots$  for an infinite cylinder). Electric field distribution has a dependence  $\Psi(r)/r$  for a sphere and a dependence  $\Psi(r)/\sqrt{r}$  for a cylinder.

Equation (4) has an exact solution for homogeneous dielectric cavity  $\epsilon(r) = \epsilon_0 = \text{constant}$ . This solution reads  $\Psi(r) = J_{\nu+1/2}(kr)$ , where  $J_{\nu+1/2}(kr)$  is the Bessel function of the first kind. The mode spectrum is determined by the boundary conditions  $\Psi(r) \rightarrow 0$  for  $r \rightarrow \infty$  and 0, where  $R$  is the radius of the sphere or cylinder. In the case of high mode order  $\nu \gg 1$ ,

$$k_{\nu, q} \approx \frac{1}{R \sqrt{\epsilon_0}} \left[ \nu + \alpha_q \left( \frac{\nu}{2} \right)^{1/3} - \left( \frac{\epsilon_0}{\epsilon_0 - 1} \right)^{1/2} + \frac{3\alpha_q^2}{20} \left( \frac{2}{\nu} \right)^{1/3} + O(\nu^{-2/3}) \right], \quad (5)$$

where  $\alpha_q$  is the  $q$ th root of the Airy function,  $Ai(-z)$ , which is equal to 2.338, 4.088, and 5.521 for  $q = 1, 2, 3$ , respectively.<sup>31</sup>

The first-order approximation for the mode eigenfunctions and eigenvalues may be found from the solution of an approximate equation:

$$\frac{\partial^2 \Psi}{\partial r'^2} + \left[ k^2 \epsilon_0 - \frac{\nu(\nu+1)}{R^2} - r' \frac{2\nu(\nu+1)}{R^3} \right] \Psi = 0, \quad (6)$$

where we assume that  $\nu \gg 1$ ,  $r' = R - r$ , and  $\Psi(0) = \Psi(R) = 0$ . Comparison of the numerical solution of

the exact equation (4) and of the approximate equation (6) shows that the solution of Eq. (6) gives satisfactory results for the eigenvalues as well as eigenfunctions of the exact problem.

To describe dispersion of the modes, we compare a value equal to the ratio of frequency separations between two pairs of neighboring modes and the mode width. The number of equidistant modes in the case of large  $\nu$  can be estimated as

$$N = \max_q \left| \left( \frac{\partial^2 k_{\nu, q}}{\partial \nu^2} \right)^{-1} \frac{k_{\nu, q}}{2Q} \right|. \quad (7)$$

From expression (5) we derive

$$N_1 \approx 1.2 \frac{\nu^{8/3}}{Q}. \quad (8)$$

The mode dispersion can be very high for realistic conditions. For example, for  $\nu = 10^3$ , cavity modes can already be treated as unequidistant for  $Q \geq 10^8$ . When one keeps in mind that the maximum-achieved quality factor for a WGM is  $9 \times 10^9$ ,<sup>3</sup> one can see that the dispersion problem is in fact quite important.

## 3. WHISPERING-GALLERY MODES IN A CAVITY MADE OF A GRADED DIELECTRIC

### A. Dispersion Compensation for the Main Mode Sequence

Let us now study the mode spectrum of a dielectric cavity with a spatially distributed refractive index:

$$\epsilon(r) = \epsilon_0 + \epsilon'(R - r). \quad (9)$$

We show in the following that by choosing a ratio between constants  $\epsilon_0$  and  $\epsilon'$  in an appropriate way one is able to suppress the mode dispersion significantly.

Exact analytical solutions of Eq. (4) with  $\epsilon(r)$  determined by Eq. (9) is rather difficult to obtain. We therefore simplify the problem by assuming that the radius of the cavity is large enough,  $R \gg \lambda$ , where  $\lambda$  is the optical wavelength in the material. In this case  $\nu \gg 1$ , and almost all the energy of the mode is confined near the surface of the cavity in a layer having a thickness  $\sim R\nu^{-2/3}$ . Introducing  $r' = R - r$ , we decompose Eq. (4), assuming that  $1 \gg r'/R$ :

$$\frac{\partial^2 \Psi}{\partial r'^2} + \left\{ \left[ k^2 \epsilon_0 - \frac{\nu(\nu+1)}{R^2} \right] - r' \left[ \frac{2\nu(\nu+1)}{R^3} - k^2 \epsilon' \right] \right\} \Psi = 0. \quad (10)$$

This equation has an exact solution:

$$\Psi_q(r') = \Psi_{q,0} Ai \left\{ \left[ \frac{2\nu(\nu+1)}{R^3} - k_q^2 \epsilon' \right]^{1/3} \frac{r'}{\alpha_q} - \alpha_q \right\}, \quad (11)$$

where  $\Psi_{q,0}$  is the field amplitude and  $k_q$  is the root of the equation

$$k_q^2 \epsilon_0 - \frac{\nu(\nu+1)}{R^2} = \alpha_q \left[ \frac{2\nu(\nu+1)}{R^3} - k_q^2 \epsilon' \right]^{2/3}. \quad (12)$$

It is easy to see that Eq. (12) gives a close approximation of the first two terms of the decomposition [expression (5)] if  $\epsilon' = 0$ . For nonzero  $\epsilon'$  we get

$$k_{\nu,q} \approx \frac{1}{R\sqrt{\epsilon_0}} \left[ \nu + \alpha_q \left( \frac{\nu}{2} \right)^{1/3} \left( 1 - \frac{R}{2} \frac{\epsilon'}{\epsilon_0} \right)^{2/3} \right]. \quad (13)$$

The number of equidistant modes for the cavity can be found from Eq. (7) and expression (13):

$$N_2 \approx 1.2 \frac{\nu^{8/3}}{Q} \left( 1 - \frac{R}{2} \frac{\epsilon'}{\epsilon_0} \right)^{-2/3}. \quad (14)$$

Therefore, if  $\epsilon' \rightarrow 2\epsilon_0/R$ , the cavity has, to the first order, an equidistant frequency spectrum. Our numerical solution of the exact problem, presented in Fig. 1, confirms the results derived from the analytical solution.

### B. Dispersion Compensation for the Radial Mode Spectrum

Surprisingly, except for  $\nu$ -dispersion compensation, a graded material cavity demonstrates radial dispersion compensation (index  $q$ ) (Fig. 2). This happens because modes do not encounter the cavity boundaries for large refractive-index gradients but only the potential dip created owing to the gradient. As a consequence, radial profiles of cavity modes are nearly symmetrical, much in the same way as harmonic-oscillator wave functions (see inset of Fig. 2).

This conclusion follows from complex-angular-momentum theory.<sup>32</sup> In this theory an analogy between optics and mechanics is utilized, and the cavity modes are described as eigenvalues of an effective potential  $U$ . For WGMs with index  $\nu$ , this potential may be written as a sum of an attractive wall of depth  $[\epsilon(r) - 1]k^2$  with the centrifugal potential  $\nu(\nu+1)/r^2$ .

The potential is asymmetric when  $\epsilon$  does not depend on radius  $r$  inside the sphere (see Fig. 3, solid curve). In the spheres possessing dielectric susceptibilities increasing to the sphere center, the potential pocket broadens, shifts into the cavity, and becomes more symmetric. The minimum of the potential is still on the sphere surface. For the critical value of the susceptibility gradient, the potential resembles half of the oscillatory potential  $U \sim (r - R)^2|_{r \rightarrow R-0}$  (see Fig. 3, short-dashed curve). For the

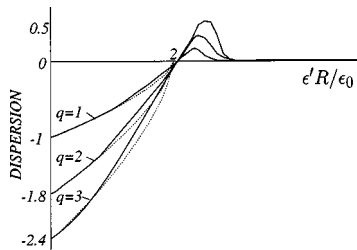


Fig. 1. Normalized second-order dispersion  $\partial^2 k_{q,\nu} / (\partial k_{q,\nu}^2)$  versus a normalized gradient of the index of refraction of the material  $\epsilon' R / \epsilon_0$  for  $\nu_0 \approx 600$ . Unity dispersion corresponds to  $|\partial^2 k_{1,\nu} / (\partial k_{1,\nu}^2)|_{\epsilon'=0}$  at  $\nu = \nu_0$ .

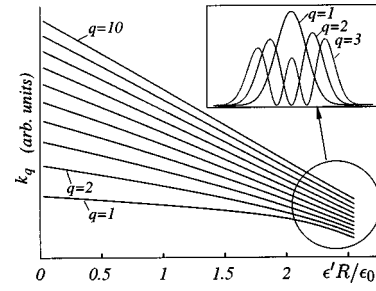


Fig. 2. Dependence of wave-vector eigenvalues  $k_{q,\nu}$  on a normalized gradient of the index of refraction  $\epsilon' R / \epsilon_0$  for  $\nu \approx 600$ . Modes with different  $q$  become closer as the gradient increases. The modes pushed far away from the cavity boundary are nearly equidistant. Inset: amplitude profile for the fields for large index gradients. The mode wave functions are nearly symmetric.

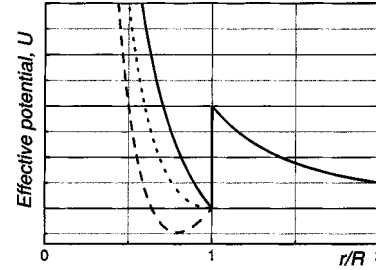


Fig. 3. Effective optical potential  $U$  for a transparent dielectric resonator with radius  $R$ . Solid curve,  $\epsilon(r) = \text{const.}$  ( $R > r$ ); short-dashed curve,  $\epsilon(r) = \epsilon_0(3 - 2r/R)$  (critical gradient); long-dashed curve,  $\epsilon(r) = \epsilon_0(5 - 4r/R)$ .

gradients beyond the critical value, the minimum of the potential moves into the cavity. The deeper the minimum of the potential is, the better it can be described by the oscillatory potential (Fig. 3, long-dashed curve).

### C. Engineering the Cavity Field Distribution for Improving Mode Quality Factors

The gradient in the index of refraction affects the field distribution in the cavity. By increasing  $\epsilon'$ , we push the WGMs further into the resonator [Eq. (11)] (Fig. 4). This might greatly reduce the losses caused by surface defects such as dust or scratches. The change of the mode geometry also changes cavity radiative losses.<sup>29</sup> However, because radiative losses are usually insignificant compared with the losses that are due to surface scattering, we do not consider radiative losses here.

Moreover, an efficient coupling with WGMs may be achieved by a prism or fiber coupler that is in physical contact with the dielectric cavity. This may significantly simplify usage of WGM cavities outside a laboratory. Such a contact usually overloads the modes of a dielectric cavity and results in a significant broadening of the resonances. However, by engineering the profile of the dielectric susceptibility gradient, we reduce the evanescent field of the cavity in such a way that the coupling is still possible, but the influence of the surface contamination is greatly suppressed.

Usually, the quality factor of a WGM is determined by three effects: absorption in the material,  $Q_m$ ; surface scattering losses,  $Q_{ss}$ ; and loading by the external coupler,  $Q_l$ . The load quality factor can be regulated from

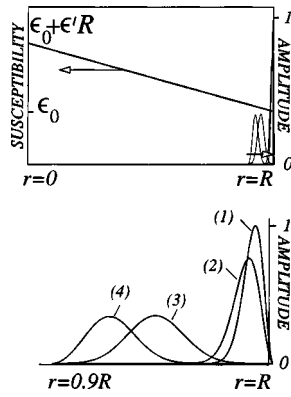


Fig. 4. Radial dependencies of the susceptibility of a cavity material as well as of the amplitude profiles of the field ( $q = 1$ ) inside the cavity for various  $\epsilon'$ . Top, real scale for the field distributions in the case of  $\nu_0 = 600$ . The fields are localized close to the cavity surface. Bottom, amplitude profiles in detail. Curve (1) of the bottom plot corresponds to  $\epsilon' R / \epsilon_0 = 0$ , curve (2) to  $\epsilon' R / \epsilon_0 = 1$ , curve (3) to  $\epsilon' R / \epsilon_0 = 2$ , and curve (4) to  $\epsilon' R / \epsilon_0 = 2.4$ . It is easy to observe the pushing of the mode out of the cavity boundary ( $r = R$ ) and into the cavity.

outside. It depends on the distance,  $d$ , from the coupling prism to the sphere surface as follows:

$$Q_l \sim \exp\left(\frac{4\pi d \sqrt{\epsilon_0 - 1}}{\lambda}\right), \quad (15)$$

where  $\lambda$  is the mode wavelength. The critical (optimum) coupling with the mode is achieved if  $d$  is chosen such that  $Q_l = (1/Q_{ss} + 1/Q_m)^{-1}$ . Because usually  $Q_m \gg Q_{ss}$ , one neglects the absorption of the material.

Both  $Q_{ss}$  and  $Q_l$  are proportional to the ratio of the field power on the surface of the cavity and the total energy of the mode.<sup>33</sup> In other words, one can present the power of the losses because of the surface scattering and because of the coupler as  $P_{ss} = \beta E(r = R)^2$  and  $P_l = \alpha E(r = R)^2$ , respectively, where  $\alpha$  is a geometrical factor that depends on the shape and the dielectric constants of a coupler and a thin surface layer in which the WGM is localized and on the distance between the coupler and the cavity surface;  $\beta$  depends on the geometry of the surface inhomogeneities and their optical parameters; and  $E(r = R)$  is the amplitude of the electric field on the cavity surface.

The quality factor may be determined as  $Q_{l,ss} = W/(P_{l,ss}T)$ , where  $W$  is the energy stored in the mode and  $T$  is the oscillation period. By changing the profile of the index of refraction  $\epsilon(r)$ , we change the ratio  $W/E(r = R)^2$ , but  $Q_l/Q_{ss}$  stays unchanged. Therefore, by choosing  $Q_l/Q_{ss} = 1/2$  and reducing the absorption that is due to the surface scattering via engineering a cavity index of refraction such that  $Q_{ss} = Q_m$ , we may reach both the critical coupling and the maximum index of refraction. The maximum achievable quality factors for silica microspheres are approximately  $Q_m = 10^{12}$ .<sup>33</sup>

For instance, to estimate the increase of the quality factors with the index gradient, it is convenient to use a simple ratio. Let us consider two identical spherical microcavities except that the susceptibility of one cavity is

constant  $\epsilon_0$  and the susceptibility of the other is space-dependent  $\epsilon(r)$  [ $\epsilon(R) = \epsilon_0$ ]. The ratio of the quality factors of the cavities is

$$\frac{Q_l}{\tilde{Q}_l} \approx \frac{Q_{ss}}{\tilde{Q}_{ss}} \approx \frac{\psi^2(r = R) R(\epsilon_0 - 1)}{\int_0^R \Psi^2(r) dr \frac{2\epsilon_0}{2\epsilon_0}}, \quad (16)$$

where  $Q_l$  and  $Q_{ss}$  ( $\tilde{Q}_l$  and  $\tilde{Q}_{ss}$ ) are the quality factors that are due to loading and surface scattering for the cavity with constant (graded) susceptibility and  $\Psi(r) \sim E(r)$  is the field distribution of a TE mode of the dielectric cavity  $\Psi(r = R)$  (the deeper is the mode localization), the less are the absorption and coupling and the higher the quality factors. The dependence is shown in Fig. 5.

Finally, let us consider a situation in which a coupling prism is in full contact with the dielectric cavity ( $d = 0$ ). The coupling losses exceed the surface scattering losses in this case. We may increase  $Q_l$ , changing  $\epsilon(r)$  until the bulk optical losses become equal to the coupling losses. At this point we have critical coupling but at a much higher  $Q$ -factor level.

It is worth noting here that in some cases it is important to increase the evanescent field of a dielectric cavity, not to decrease it, as we discussed above. One example is if the cavity is intended to be used as an optical sensor. This problem may also be managed via manipulation of  $\epsilon(r)$  dependence. It has been shown that WGMs tend to be closer to the cavity surface if the index of refraction of the cavity close to its surface exceeds the internal index of refraction.<sup>29</sup> Such dependence of the refractive index will increase the surface absorption, but it will also increase the coupling to the external space.

#### D. Numerical Simulations

Our approximation  $1 \gg r'/R$  breaks down for  $\epsilon' \rightarrow 2\epsilon_0/R$ , so we are unable to infer the extent of the dispersion compensation and reshaping of the mode from these analytical calculations. Our exact numerical simulations show that the approximate analytical solution gives rather satisfactory results for the gradients less than the critical value.

Let us now solve the exact equation (4) with boundary conditions  $\Psi(r = 0) = 0$  and  $\Psi(r \rightarrow \infty) = 0$  numerically.

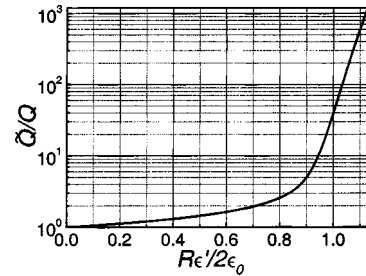


Fig. 5. Quality factor  $\tilde{Q}$  of a cavity with a gradient of the refractive index normalized by the quality factor  $Q$  of a cavity of the same radius without the gradient versus a normalized gradient of the refractive index. The plot is created for a cavity with radius  $R = 4$  mm, susceptibility  $\epsilon_0 = 2.1$ , and mode wavelength  $\lambda = 1.55$   $\mu\text{m}$ .

The result is presented in Figs. 1 and 2. The second-order dispersion versus gradient of the refractive index is shown in Fig. 1. This dispersion determines the number of equidistant modes  $N$  [Eq. (7)]. It is easy to see a good correspondence between the eigenvalues of the exact equation (4) (solid curves) and the first-order approximation of this equation [Eq. (10)] (dotted curves). It is important to note that in the region  $\epsilon' \geq 2\epsilon_0/R$ , where Eq. (10) is not valid, the second-order dispersion becomes negative. This allows for compensation of the dispersion of the cavity host material, which is not taken into account in our calculations. Except for the complete compensation point in the vicinity of  $\epsilon' = 2\epsilon_0/R$ , the dispersion decreases and reaches a minimum of a half percent of the initial value for large gradients.

### E. Suggestions for Implementation

It is not necessary to produce a cavity that has a gradient of the index of refraction in the entire cavity. The modes of the cavity are localized in the vicinity of the cavity surface (Fig. 4). Therefore the gradient may be localized in the vicinity of the surface as well.

For example, if we build a spherical cavity of 500  $\mu\text{m}$  in radius from an optically homogeneous material and study modes with  $\nu = 10^3$  and quality factor  $Q = 10^8$ , the mode spectrum is not completely equidistant. In turn, if the same cavity is fabricated from a graded material with  $\epsilon'/\epsilon \approx 40 \text{ cm}^{-1}$  gradient of index in the vicinity of the cavity boundary  $\Delta R \approx 5 \text{ }\mu\text{m}$ , at least a hundred modes of the cavity can be treated as equidistant.

For example, there are multimode fibers with germanium-doped cores ( $\sqrt{\epsilon_0} \approx 1.5$ ) and pure silica clads ( $\sqrt{\epsilon_0} \approx 1.45$ ). Originally the fiber has steplike dependence of the refractive index on the radius. Heating of the fiber results in diffusion of the Ge ions into the clad. This results in formation of the gradient in the refractive index.

Let us consider a fiber with a 1-mm core diameter and 8- $\mu\text{m}$  clad. In this case, the gradient is closed to the critical one after thermal diffusion is realized. In addition, we may create a sphere from a high-index flint glass ( $\sqrt{\epsilon_0} \approx 1.7$ ) and cover it with fluoride glass ( $\sqrt{\epsilon_0} \approx 1.4$ ). Subsequent thermalization will allow us to create gradients that even exceed the critical one in a thick surface layer.

## 4. CONCLUSION

In conclusion, we have demonstrated that a number of important advantages can be achieved with a whispering-gallery-mode microcavity fabricated from a material with a graded index of refraction. Graded-index material is widely available in the form of lenses and fibers. Such material can be formed into microcavities with standard mechanical and thermal fusion techniques. The main advantage of the graded-index microcavity is that the spectrum of resonant frequencies is equidistant to first order. Second, the mode field is pushed away in a controlled manner from the boundary to inside the dielectric, thereby diminishing the detrimental effect of surface roughness and contamination. Finally, an appropriately engineered near-surface gradient will eliminate the need

for an adjustable (and unstable) air gap between the WGM microcavity and the evanescent coupler. This approach will be a major enhancement for a variety of applications and a significant breakthrough permitting simple packaging solutions for practical devices. We expect that ultra-high- $Q$  microcavities based on a gradient-index approach will not only enhance the performance and expand the range of applications but also provide a critical step toward their wide acceptance as a novel building block of modern photonics.

## ACKNOWLEDGMENTS

The research described in this paper was carried out by the Jet Propulsion Laboratory, California Institute of Technology, under a contract with NASA. A.A. Savchenkov also acknowledges support from National Research Council.

A. Matsko's e-mail address is andrey.matsko@jpl.nasa.gov.

## REFERENCES AND NOTES

1. V. B. Braginsky, M. L. Gorodetsky, and V. S. Ilchenko, "Quality-factor and nonlinear properties of optical whispering-gallery modes," *Phys. Lett. A* **137**, 393–397 (1989).
2. L. Collot, V. Lefevre-Seguin, M. Brune, J.-M. Raimond, and S. Haroshe, "Very high- $Q$  whispering-gallery mode resonances observed in fused silica microspheres," *Europhys. Lett.* **23**, 327–334 (1993).
3. M. L. Gorodetsky, A. A. Savchenkov, and V. S. Ilchenko, "Ultimate  $Q$  of optical microsphere resonators," *Opt. Lett.* **21**, 453–455 (1996).
4. D. W. Vernooy, V. S. Ilchenko, H. Mabuchi, E. W. Streed, and H. J. Kimble, "High- $Q$  measurements of fused-silica microspheres in the near infrared," *Opt. Lett.* **23**, 247–249 (1998).
5. H. M. Tzeng, K. F. Wall, M. B. Long, and R. K. Chang, "Laser emission from individual droplets at wavelengths corresponding to morphology-dependent resonances," *Opt. Lett.* **9**, 499–501 (1984).
6. J. C. Knight, H. S. T. Driver, R. J. Hutcheon, and G. N. Robertson, "Core-resonance capillary-fiber whispering-gallery-mode laser," *Opt. Lett.* **17**, 1280–1282 (1992).
7. A. F. J. Levi, S. L. McCall, S. J. Pearton, and R. A. Logan, "Room-temperature operation of submicrometer radius disk laser," *Electron. Lett.* **29**, 1666–1668 (1993).
8. V. Sandoghdar, F. Treussart, J. Hare, V. Lefevre-Seguin, J. M. Raimond, and S. Haroche, "Very low threshold whispering-gallery-mode microsphere laser," *Phys. Rev. A* **54**, R1777–R1780 (1996).
9. F. Treussart, V. S. Ilchenko, J. F. Roch, P. Domokos, J. Hare, V. Lefevre, J. M. Raimond, and S. Haroche, "Whispering gallery mode microlaser at liquid helium temperature," *J. Lumin.* **76**, 670–673 (1998).
10. F. Treussart, V. S. Ilchenko, J. F. Roch, J. Hare, V. Lefevre-Seguin, J. M. Raimond, and S. Haroche, "Evidence for intrinsic Kerr bistability of high- $Q$  microsphere resonators in superfluid helium," *Eur. Phys. J. D* **1**, 235–238 (1998).
11. M. Pelton and Y. Yamamoto, "Ultralow threshold laser using a single quantum dot and a microsphere cavity," *Phys. Rev. A* **59**, 2418–2421 (1999).
12. A. N. Oraevsky, M. O. Scully, T. V. Sarkisyan, and D. K. Bandy, "Using whispering gallery modes in semiconductor microdevices," *Laser Phys.* **9**, 990–1003 (1999).
13. M. Cai, O. Painter, K. J. Vahala, and P. C. Sercel, "Fiber-

- coupled microsphere laser," *Opt. Lett.* **25**, 1430–1432 (2000).
14. F. Lissillour, P. Feron, N. Dubreuil, P. Dupriez, M. Poulain, and G. M. Stephan, "Erbium-doped microspherical lasers at 1.56  $\mu\text{m}$ ," *Electron. Lett.* **36**, 1382–1384 (2000).
15. Y. S. Choi, H. J. Moon, K. Y. An, S. B. Lee, J. H. Lee, and J. S. Chang, "Ultrahigh- $Q$  microsphere dye laser based on evanescent-wave coupling," *J. Korean Phys. Soc.* **39**, 928–931 (2001).
16. D. W. Vernooy, A. Furusawa, N. P. Georgiades, V. S. Ilchenko, and H. J. Kimble, "Cavity QED with high- $Q$  whispering gallery modes," *Phys. Rev. A* **57**, R2293–R2296 (1998).
17. G. Annino, M. Cassettari, M. Fittipaldi, L. Lenci, I. Longo, M. Martinelli, C. A. Massa, and L. A. Pardi, "Whispering gallery mode dielectric resonators in EMR spectroscopy above 150 GHz: problems and perspectives," *Appl. Magn. Res.* **19**, 495–506 (2000).
18. V. S. Ilchenko, X. S. Yao, and L. Maleki, "Microsphere integration in active and passive photonics devices," in *Laser Resonators III*, A. Kudryashov and A. H. Paxton, eds., *Proc. SPIE* **3930**, 154–162 (2000).
19. V. S. Ilchenko and L. Maleki, "Novel whispering-gallery resonators for lasers, modulators, and sensors," in *Laser Resonators IV*, A. Kudryashov and A. H. Paxton, eds., *Proc. SPIE* **4270**, 120–130 (2001).
20. W. von Klitzing, R. Long, V. S. Ilchenko, J. Hare, and V. Lefevre-Seguin, "Tunable whispering gallery modes for spectroscopy and CQED experiments," *New J. Phys.* **3**, 141–144 (2001).
21. S. Blair and Y. Chen, "Resonant-enhanced evanescent-wave fluorescence biosensing with cylindrical optical cavities," *Appl. Opt.* **40**, 570–582 (2001).
22. R. W. Boyd and J. E. Heebner, "Sensitive disk resonator photonic biosensor," *Appl. Opt.* **40**, 5742–5747 (2001).
23. A. Eschmann and C. W. Gardiner, "Stability and switching in whispering gallery mode microdisk lasers," *Phys. Rev. A* **49**, 2907–2913 (1994).
24. F. C. Blom, D. R. van Dijk, H. J. W. M. Hoekstra, A. Driesen, and T. J. A. Pompa, "Experimental study of integrated-optics microcavity resonators: toward an all-optical switching device," *Appl. Phys. Lett.* **71**, 747–749 (1997).
25. J. Popp, M. H. Fields, and R. K. Chang, " $Q$  switching by saturable absorption in microdroplets: elastic scattering and laser emission," *Opt. Lett.* **22**, 1296–1298 (1997).
26. J. E. Heebner and R. W. Boyd, "Enhanced all-optical switching by use of a nonlinear fiber ring resonator," *Opt. Lett.* **24**, 847–849 (1999).
27. V. V. Klimov, M. Ducloy, and V. S. Letokhov, "Strong interaction between a two-level atom and the whispering-gallery modes of a dielectric microsphere: quantum-mechanical consideration," *Phys. Rev. A* **59**, 2996–3014 (1999).
28. V. S. Ilchenko, M. L. Gorodetsky, X. S. Yao, and L. Maleki, "Microtorus: a high-finesse microcavity with whispering-gallery modes," *Opt. Lett.* **26**, 256–258 (2001).
29. D. Q. Chowdhury, S. C. Hill, and P. W. Barber, "Morphology-dependent resonances in radially inhomogeneous spheres," *J. Opt. Soc. Am. A* **8**, 1702–1705 (1991).
30. The equation for TM modes looks similar; however, we do not consider it here for the sake of clarity.
31. C. C. Lam, P. T. Leung, and K. Young, "Explicit asymptotic formulas for the positions, widths, and strengths of resonances in Mie scattering," *J. Opt. Soc. Am. B* **9**, 1585–1592 (1992).
32. L. G. Guimaraes and H. M. Nussenzveig, "Theory of Mie resonances and ripple fluctuations," *Opt. Commun.* **89**, 363–369 (1992).
33. M. L. Gorodetsky, A. D. Pryamikov, and V. S. Ilchenko, "Rayleigh scattering in high- $Q$  microspheres," *J. Opt. Soc. Am. B* **17**, 1051–1057 (2000).